NASA TECHNICAL MEMORANDUM

NASA TM X-67840

NASA TM X-67840

SUPERSONIC COMBUSTION OF HYDROGEN IN A VITIATED AIR STREAM USING STEPPED-WALL INJECTION

by M. C. Burrows and A. P. Kurkov
Lewis Research Center
Cleveland, Ohio

TECHNICAL PAPER proposed for presentation at Seventh Propulsion Joint Specialist Conference sponsored by the American Institute of Aeronautics and Astronautics
Salt Lake City, Utah, June 14-18, 1971

SUPERSONIC COMBUSTION OF HYDROGEN IN A VITIATED AIR STREAM USING STEPPED-WALL INJECTION

M. C. Burrows and A. P. Kurkov

Lewis Research Center
National Aeronautics and Space Administration
Cleveland, Ohio

Abstract

Detailed probe measurements of temperature, pressure, and composition were taken within a two-dimensional test section. A high pressure gas generator supplied Mach 2.5 vitiated air or inert gas at elevated temperatures. Special water-cooled probes and sampling techniques were developed for the short test times required by heat-sink hardware. Independent methods of measuring stream total temperatures are compared. The mixing boundary of hydrogen with the supersonic gas stream was substantially wider in the presence of combustion. Ignition of hydrogen, as determined from photographic exposures of the radiating gases, varied from 31 cm downstream from injection to 11 cm for a 20°K variation in stream static temperature. Ignition times correspond to literature values for lean mixtures.

E-6319

Introduction

The design of supersonic combustors for advanced air-breathing engines requires experimental data on the diffusive mixing and reaction of fuel and air at the high temperatures typical for flight Mach numbers above 6. The mixing of hydrogen with the supersonic air stream has generally been by one of several different experimental configurations: parallel or angled flow from a stepped wall through a slot configuration, and normal or angled flow of hydrogen through arrays of holes of various aspect ratios, reference 1.

Parallel stepped-wall injection of hydrogen into the combustor is attractive for detailed experimental study since it results in minimum disturbance of the free stream when fuel and air pressures are matched. Two-dimensional flow lends itself readily to studies of ignition delay and mixing lengths, and can be compared with analytical models.

Current techniques of generating a supersonic air stream for combustor testing requires an arc heater, storage heater, combustion device, or a combination of the methods. The arc heater and storage heater have the advantage of adding no water vapor to the air stream, but small particulate matter can be entrained in the air from the heater elements.

In the tests reported herein, the high temperature gas stream was produced by burning a hydrogen-nitrogen gas mixture with liquid oxygen at high pressure. Each component was regulated so that the desired total temperature was achieved with an oxygen content in the vitiated air stream of about 21 percent by volume. For the non-reacting mixing tests, the gas products contained no oxygen and only a small fraction of hydrogen, similar to the method in reference 2. The balance in both cases was composed of nitrogen and water vapor.

The objective of this work was to obtain detailed measurements which were necessary to construct the flow field at stations downstream from the injection point of hydrogen. Cases included hydrogen burning with vitiated air and hydrogen mixing with hot, inert gas products.

The instrumentation developed for gas temperature, pitot pressure, and gas sampling measurements is discussed. Temperatures measured by a thermocouple probe are compared with those measured indirectly with a cooled-gas pyrometer, reference 3. Composition profiles for hydrogen burning with vitiated air and hydrogen mixing with hot, inert gas products show the changes caused by combustion. Complete profiles of static pressure, static temperature, Mach number, velocity, and composition for burning and nonburning cases are presented.

Ignition time is determined as a function of local static temperature. Calculated values are compared with published induction times.

Experimental Hardware

Gas generator. - An overall view of the experimental hardware is shown in figure 1. The high-pressure, heat-sink combustion chamber was constructed of electrolytic copper. The internal cross section of the chamber was 5.1 cm x 9.53 cm and its length was 40.6 cm. A 36-element concentric tube injector was used for uniform introduction and mixing of the propellants.

The combustion efficiency, as determined by characteristic exhaust velocity, was approximately 96 percent. The remaining 4 percent was attributed to heat transfer to the inner surfaces of the chamber. A more uniform temperature distribution was achieved by inserting two 1.95 cm diameter copper bars at different axial locations in the chamber.

The two dimensional copper nozzle was designed to supply parallel flow to the test section at Mach 2.5 and atmospheric pressure. Particular care was taken to match the 5.1 cm x 8.9 cm nozzle exit to the test section walls so that no change in area occurred between them. The total temperature profile at the entrance to the test section is shown in figure 2. The values are ratioed to the equilibrium gas temperature calculated from propellant mass flows, T_{ref}.

Test section. - The test section, figure 3, was constructed of four machined copper plates which were bolted together and matched with the nozzle exit. The cross section, which included the nickel injector on one wall, remained constant to the step. Thereafter the test section expanded linearly from 5.1 cm x 9.38 cm to 5.1 cm x 10.5 cm at the exit to compensate for the boundary layer build-up.

Hydrogen was injected into the test section through the backward-facing step at Mach 1, atmospheric pressure, and parallel to the vitiated air flow. Lip thickness at the top of the step was .076 cm. Seven ribs across the 5.1 cm width, each .076 cm thick, straightened the flow and prevented warpage of the top plate and lip. The total temperature of the hydrogen flowing through the slot could be varied from 300K to 800K. Hydrogen was heated in a storage heater which contained a coil of heavy-walled stainless steel pipe embedded in a 4.5 Kw electric furnace.

Static pressure taps were spaced at 1.25 cm to 3.8 cm increments along the wall downstream from the step and monitored with a multiple - scanning pressure transducer. Four 15.1 cm diameter quartz windows were mounted flush with the inner wall surfaces for visual and photographic observations within the test section.

Thermocouple and pitot pressure probes. - A water-cooled, wedge shaped thermocouple probe was designed with a blunted leading edge, figure 4A. The exposed-junction thermocouple could be easily replaced in case of tip failure. Thermocouple materials were iridium--iridium/40 percent rhodium or tungsten--tungsten/26 percent rhenium. Wire diameters ranged from .025 cm to .076 cm. A similar water-cooled probe was constructed for pitot pressure measurements. The pressure port was located in the leading edge of the probe approximately.2 cm from the end.

In the boundary layer and in the low temperature hydrogen-rich mixing region, miniature swaged thermocouples and miniature pitot pressure probes were used.

Sampling probes. - Two similar water-cooled probes were designed to obtain gas samples and were also used for indirect temperature measurements. The first probe, designated as Probe I, could be extended into the test section closer to the step. The second probe, designated as Probe II, figure 4B, could only be used in the test section exit plane. The copper cone tip in this probe is replaceable.

The two sampling probe tips are shown in figure 5A and 5B. In Probe I, water was supplied through circumferentially placed tubes and returned through the annular spaces between the tubes. Water in Probe II was dumped downstream from the tip. Probe I also incorporated 3 static pressure taps spaced equally around the cone surface .635 cm downstream from the probe tip.

Both Probes I and II were fitted with a small venturi 15.4 cm and 11.8 cm downstream respectively. Each venturi was instrumented with two pressure taps and a small thermocouple. A second venturi was placed downstream between the probe sample outlet and the sample container, and was also equipped with pressure taps and a thermocouple. The amount of water vapor in each trapped sample was deduced from the difference in the hot and cooled gas mass flows, after adjusting for saturated gas flow in the second venturi. The water droplets which collected on the inner wall of the sample line were purged out with helium before each succeeding run.

The sampling probes were also used as a cooled gas pyrometer to indirectly measure the stream total temperature, and a pitot pressure probe.

Experimental Procedure

Runs were sequenced for a three second duration with steady state flows established for 2.5 seconds or longer. Motion picture analysis verified stability of the combustion process above the ignition limits. Generally, all readings were taken 2.5 seconds after initiation of each run. Instrumentation probes used in the test section were moved incrementally between succeeding runs to obtain the profiles of pitot pressure, total temperature, and composition.

Static pressures were measured at the entrance to the test section, along the wall downstream from the hydrogen injection step, in the gas generator, and upstream from the sonic-flow nozzles in the nitrogen and hydrogen supply lines.

Precision and Reproducibility of Measurements

Gas generator flows were reproducible within $\pm$ 1 percent. The Mach number distribution in the test section proved to be uniform within 3 percent in a 6 cm core section before the step. Pressure, temperature, and composition measurements were generally within a band of $\pm$ 2.5 percent. In the reaction zone, measurements varied over a wider range from run to run.

Temperatures indicated by the thermocouple probe were reproducible within $\pm$ 3 percent when care was taken to insure integrity of wire, junction, and alumina insulator. Readings were taken after junction temperature had stabilized, similar to the procedure in reference 4.

The sampling probes were calibrated with reference flow nozzles over a range of flows corresponding to the Reynolds number range encountered in the test runs. Heat transfer characteristics of each probe were obtained using heated nitrogen. Analysis of the trapped samples was done on a mass spectrometer and on a dry basis, were accurate within 2 percent. Water vapor fraction depended upon the difference in the two nozzle flows, and was estimated to be within $\pm$ 5 percent.

Results and Discussion

Experimental conditions. - The measurements in the combustion region were obtained for approximate free stream conditions at the entrance to the test section of Mach 2.5, atmospheric pressure, and static temperature generally in the range 1200K to 1220K. In the pure mixing case, the Mach number and static pressure were about the same while the static temperature was slightly lower, or about 1150K. In both cases, hydrogen was injected at sonic velocity, matched static pressure, and a total temperature which was slightly above ambient temperature in most cases. These input conditions will be assumed to apply to the data unless other conditions are specifically stated.

The majority of results were obtained at the test section exit plane 35.6 cm downstream from the hydrogen injection step. Hence in reporting

the results, this station will be implied unless otherwise noted. The thermocouple probe and pitot pressure probe were receded slightly from the test section exit plane to ensure that the detached shock off the probe leading edge does not extend inside the test section.

Composition measurements. - Originally the composition profile for the reacting case was calculated from the sampling data obtained using Probe I and shown in figure 6. However, it is believed that some of the water condensed upstream from the probe venturi for data points taken in the exit plane between Y = 0 and Y = 1.75 cm, where stream temperature was relatively low. This conclusion was reached since the cooled-gas pyrometer total temperature fell considerably below the total temperature obtained directly using the thermocouple probe. Apparently the cooling water temperature did not increase sufficiently to prevent condensation on the thermocouple wires. The thermocouple reading therefore did not correspond to the true temperature. However, the composition in the free stream region agreed well with the average composition of vitiated air calculated from the measured propellant flows.

The sampling traverse was repeated with the probe cooling water preheated nearly to the boiling point. It was necessary to use another probe for this traverse, Probe II, because the tip of Probe I developed a water leak. The composition profile calculated from Probe II measurements is shown in figure 7. In comparison with the previous figure, the water vapor volume fraction is considerably reduced for Y less than 2 cm. The higher water content in this region in figure 6 results from the fact that the mass flow rate through the probe venturi was based on a thermocouple temperature which was actually lower than the true gas temperature due to condensation effects.

In calculating the mass flow through the probe venturi, it was assumed that the gas bulk temperature, T_l, is related to the measured thermocouple temperature, T_m, according to the relation:

$$T_l = T_m \left[1 - .21(T_m - T_{wl})/T_m\right] \qquad (1)$$

where T_{wl} is the tube wall temperature which is taken to be equal to the cooling water temperature. This follows from the velocity profile given in reference 5 and the assumption that the velocity and temperature profiles are similar. A similar conclusion is also reached from the data presented in reference 6.

The transport properties of the gaseous mixture, which are necessary for the determination of the Reynolds and Prandtl numbers, were calculated using approximate relations essentially identical to those presented in reference 7. Collision cross section data were obtained from reference 8.

Both oxygen and hydrogen are present in small amounts in a narrow region around Y = 2.3 cm, figure 7. Composition variations during the run or partial quenching of the chemical reactions can account for this. The mixing boundary extends approximately to 2.9 cm.

The composition profile for the nonreacting case is presented in figure 8. In this case gas samples were taken using the pitot pressure probe and consequently measurements of the sample water content were not made. It was assumed that the ratio of volume fractions of water vapor and nitrogen is constant. The mixing boundary extends about 2.3 cm from the stepped wall.

Pitot pressure measurement. - The pitot pressure measurements are presented in figure 9. The reference pressure noted in this figure was taken to be equal to the gas generator pressure. In this way, run-to-run variations in pitot pressure due to slight changes in propellant flows are reduced. The initial boundary layer thickness is about 1 cm while the width of the disturbed region is about 2.4 cm for the pure mixing case, and about 3.1 cm for the reacting case. These values are close to the boundaries determined from the composition profiles. Pitot pressures in the combustion region varied considerably during the run, indicating some fluctuation in the combustion process.

Direct total temperature measurement. - Most of the measurements were made using iridium--iridium/40 percent rhodium bare wire thermocouples and are shown in figure 10. The radiation correction was made according to the equations presented in references 9 and 10. The emissivity of the iridium and the iridium-rhodium alloy was assumed equal to the emissivity of platinum (reference 11). The emissivity data were obtained from reference 12.

The recovery correction was estimated from the results obtained for similar type thermocouples in references 13 and 14. The radiation correction did not exceed 85K while the maximum recovery correction was about 70K.

The points close to the stepped wall for X = 0 and X = 18.3 cm and the two points at X = 33 cm were obtained using miniature thermocouples. The flagged point for Y = 1.9 cm at the test section exit was obtained using a tungsten--tungsten/26 percent rhenium thermocouple. It should be noted that the indicated temperature for this point could be in error because of oxidation of the thermocouple surface. However, examination of gas composition in figure 7 indicates that only a small amount of oxygen is likely to be present at this position. It is also noted that at a somewhat lower free stream temperature, for the position of Y = 1.59 cm, the temperature obtained with a tungsten-rhenium alloy thermocouple agreed well with the value obtained at the same position using an iridium-rhodium alloy thermocouple.

Comparing the results in figures 7 and 10, it appears that the position of the maximum temperature is shifted slightly to the left of the point where water vapor fraction is a maximum.

The reference temperature, used to ratio the values of total temperature in figure 10, is the calculated gas generator temperature for each particular run. Its representative average value is noted in the legend.

Indirect total temperature measurement. - The total temperature was also calculated from the measurement of the gas sample temperature at the

probe venturi using Probes I and II as cooled-gas pyrometers, reference 3.

The bulk cooled-gas temperature, T_1, is related to the total temperature at the probe entrance, T_0, by the equation:

$$T_0 = (T_1 - T_w) \exp\left[(4X_t/d)St\right] + T_w \qquad (2)$$

where T_w is the average tube wall temperature and is assumed equal to the average water temperature; X_t is the probe thermocouple location measured from the probe tip; d is the inside diameter of the tube; and St is the Stanton number.

The Stanton number is given as a function of Reynolds number, Re, and Prandtl number, Pr, by the relation (ref. 12, 15):

$$St = H_c Re^{-a} Pr^{-.667} \qquad (3)$$

where H_c and a are constants which are determined by calibration. The Prandtl number and the viscosity in the Reynolds number were calculated for an average film temperature, T_f, which was given by the equation:

$$T_f = \left[(T_1 + T_0)/2 + T_w\right]/2 \qquad (4)$$

Probes I and II were calibrated using the total temperatures obtained from direct thermocouple probe measurements in the test section and using the data obtained in a special calibration using preheated nitrogen. The results for Probe I are shown in figure 11A. Points obtained from hydrogen-vitiated air runs in the low Reynolds number region ($Y < 1.59$ cm) were omitted in determining H_c because of the probable water vapor condensation in the probe.

The corresponding results for Probe II are shown in figure 11B. The points which fell above the $H_c = .067$ line in the low Reynolds number region were all taken for small values of Y, as seen in figure 12. In this region near the stepped wall, it is believed that the thermocouple temperatures were in error because of the boundary layer separation induced by the thermocouple probe. This is substantiated in figure 10, where two points at X = 33 cm taken with a miniature thermocouple fell considerably below the points at the 35.6 cm measuring station, verifying that the latter points were in error.

The flagged points in figures 11B and 12 deviate markedly from the $H_c = .067$ line. They fall just to the left and to the right of the maximum temperature region. (The measured temperature using the tungsten-rhenium alloy thermocouple was not included.) One reason for the deviation in H_c may be due to the different flow regime in this low Reynolds number and high temperature region. In this case there is some justification for assuming a local calibration line $H_c = .055$ for the positions which lie between the flagged points. There is, however, less justification for this assumption if the deviation of H_c is due to chemical reactions within the tip of the probe. Nevertheless, if the above two values of H_c are used to calculate the total temperatures, the results are as shown in figure 13. Also included in this figure are temperatures which were computed from measurements made using Probe I. However, Probe I points in the hydrogen-rich region were not included because of the condensation effects noted previously.

For the purpose of comparison, figure 13 also includes curves reproduced from figure 10. The dotted line close to the stepped wall passes through the cooled gas pyrometer points. It also coincides with the two points measured with the miniature thermocouple at the X = 33 cm station, figure 10. In general, a fair agreement is noted for total temperatures derived by two different methods. The cooled gas pyrometer using Probe I gives somewhat higher values in the reaction region for the hydrogen-vitiated air case and in a portion of the mixing region for the pure mixing case.

Wall static pressure measurements. - The static pressure along the stepped wall ratioed to the nozzle exit static pressure is shown plotted in figure 14. There is evidence of a slight expansion at X = 2 cm and a subsequent recompression near X = 8 cm for both the pure mixing and combustion cases. These pressure waves were not affected by a change in hydrogen injection pressure and hence must originate from a slight mismatch in the tunnel walls. Changes in hydrogen injection pressure affected only the first static pressure port, X = .58 cm. For the combustion case, the static pressure rise commencing at about 18 cm is attributed to combustion.

Temperature effects on ignition. - The ignition lengths were determined from photographs of the radiation which originated at various distances downstream from the hydrogen injection point. A fast (ASA 400) ultraviolet sensitive film was exposed for 1/15th second at f/4.5 near the end of each run. The ignition lengths as determined by the onset of ultraviolet radiation are shown in figure 15. The free stream static temperature at each data point was linearly interpolated between entrance and exit static temperatures. The ignition length increased linearly with a slight decrease in local static temperature and was not affected by a 400K change in total hydrogen temperature.

The degree of reaction can also be determined from the rise in static pressure as was shown in figure 14. The static pressure profiles for a 700K hydrogen temperature and a series of free stream static temperatures are shown in figure 16. The solid points represent ignition distances from figure 15. An increase in static pressure due to combustion occurred somewhat before onset of ultraviolet radiation. Although total static pressure rise was a function of static temperature, ignition positions could not be determined using pressure data.

Computed flow field. - The complete flow field at the test section exit plane was first calculated assuming that static pressure was uniform and equal to the wall static pressure at the 33 cm station. The composition corresponded to the plotted values in figure 7 while the total temperature and pitot pressure were obtained from faired curves in figures 13 and 9 respectively. The static pressure on the cone surface was then calculated for the positions indicated in Table I and compared with the measured cone static values. This iterative procedure on stream static pressure was repeated until calculated and measured values

of cone static pressures agreed. Table I lists the final values of static pressure in the free stream region. For final computation of the flow field, the static pressure value in the right column of Table I was used as a representative value for each test.

The cone flow solution described above was obtained for the geometry as shown in figure 5A using rotational characteristics theory. Caloric imperfections have been included in the calculations.

Mach number, static temperature, and velocity distribution at the exit station are shown in figures 17, 18, and 19. In obtaining the results plotted in these figures, the composition was assumed given by the faired curve in figure 7, rather than by the actual measured values at each location.

In the combustion region, the Mach number is significantly lower than in the pure mixing case, although the flow is still supersonic. A steep increase in static temperature is also noted in this region while the velocity remains fairly uniform. The uniformity of velocities also implies a relatively low value of the turbulent mixing intensity.

Earlier in this discussion, it was noted that the mixing-reaction region for the combustion case is significantly wider than the mixing region in the pure mixing case. This effect, however, may be largely due to the expansion of streamlines during combustion. The question of whether or not combustion enhances mixing should, therefore, be approached by using the turbulent mixing model developed for pure mixing data in a complete solution involving chemical reactions. These results should then be compared with experimental combustion data.

Induction time. - Based on the ignition tests shown in figure 15, it is possible to estimate the induction distances and compare them with published results. Since a 400K change in hydrogen total temperature did not affect the ignition limits, it was assumed that ignition originated in a region close to free stream conditions, in a lean mixture range.

For an average local static temperature of 1265K, free stream velocity of 1600 m/sec., and ignition distances from 10 cm to 30 cm, induction times ranged from 69×10^{-6} sec. to 207×10^{-6} sec. Induction times reported in reference 16 for lean hydrogen-oxygen mixtures varied from 69×10^{-6} sec. to 333×10^{-6} sec. for $(H_2)/(O_2)$ ratios between .064 and .0075 respectively. From this agreement it appears that ignition does originate in a lean H_2-vitiated air range where hydrogen volume fraction is less than .0133. Also the presence of a relatively high volume fraction of water vapor did not have a large effect on the induction times observed in these tests.

Conclusions

Complete profiles of total temperature, pitot pressure, and gas composition were taken across a two-dimensional supersonic test section. The experimental results presented here are complete at the exit station for hydrogen injected parallel to the free stream and at matched static pressure. Data are presented for the case of hydrogen burning with vitiated air, and the case of hydrogen mixing with hot, inert gas products. The width of the mixing-reaction region in the combustion case was found to be significantly greater than the mixing region width for the pure mixing case. In the center of the combustion region, Mach number decreased one-third, static temperature more than doubled, and velocity increased slightly from values for the pure mixing case. Induction times computed from the measured distances and free stream velocity agreed with the values reported in the literature for lean mixtures.

References

1. Schetz, J. A., Gilreath, H. E., and Lubard, S. C., "Fuel Injection and Mixing in a Supersonic Stream," Twelfth Symposium (International) on Combustion, Combustion Institute, Pittsburgh, 1969, pp. 1141-1149.

2. Cohen, L. S. and Guile, R. N., "Measurements in Free Jet Mixing/Combustion Flows," Paper 69-538, June 1969, AIAA, New York, N. Y.

3. Krause, L. N., Johnson, R. C., and Glawe, G. E., "A Cooled-Gas Pyrometer for Use in High-Temperature Gas Streams," TN 4383, 1958, NACA, Cleveland, Ohio.

4. Burrows, M. C., "Thermometric Determination of Oxidant-Fuel Distribution Within a Rocket Combustor," TN D-5626, 1970, NASA, Cleveland, Ohio.

5. Schlichting, H., Boundary Layer Theory, McGraw-Hill, New York, 1955, pp. 502-508.

6. Eckert, E. R. G., Introduction to the Transfer of Heat and Mass, McGraw-Hill, New York, 1950, p. 125.

7. Brokaw, R. S., "Alignment Charts for Transport Properties Viscosity, Thermal Conductivity, and Diffusion Coefficients for Nonpolar Gases and Gas Mixtures at Low Density," TR R-81, 1961, NASA, Cleveland, Ohio.

8. Svehla, R. A., Personal Communication.

9. Scadron, M. D., Warshawsky, I., and Gettelman, C. C., "Thermocouples for Jet-Engine Gas Temperature Measurements," ISA Proceedings, Vol. 7, 1952, pp. 142-148.

10. Glawe, G. E., Simmons, F. S., and Stickney, T. M., "Radiation and Recovery Corrections and Time Constants of Several Chromel-Alumel Thermocouple Probes in High-Temperature, High-Velocity Gas Streams," TN 3766, 1956, NACA, Cleveland, Ohio.

11. Glawe, G. E., Johnson, R. C., and Krause, L. N., "Intercomparison of Several Pyrometers in a High-Temperature Gas Stream," Temperature - Its Measurement and Control in Science and Industry, Vol. 3, Part 2, Reinhold, New York, 1962, pp. 601-605.

12. McAdams, W. H., Heat Transmission, 3rd ed., McGraw-Hill, New York, 1954.

13. Simmons, F. S., "Recovery Corrections for Butt-Welded, Straight-Wire Thermocouples in High-Velocity, High-Temperature Gas Streams," RM E54G22a, 1954, NACA, Cleveland, Ohio.

14. Stickney, T. M., "Recovery and Time-Response Characteristics of Six Thermocouple Probes in Subsonic and Supersonic Flow," TN 3455, 1955, NACA, Cleveland, Ohio.

15. Kreith, F., Principles of Heat Transfer, International Textbook, Scranton, 1958, pp. 346-347.

16. White, D. R. and Moore, G. E., "Structure of Gaseous Detonation. IV Induction Zone Studies in H_2-O_2 and CO-O_2 Mixtures," Tenth Symposium (International) on Combustion, Combustion Institute, Pittsburgh, 1965, pp. 785-795.

TABLE I STATIC PRESSURE IN FREE STREAM REGION

Case	Probe Position (cm)	Static Pressure	
		Local (N/m^2)	Assumed (N/m^2)
Reacting	3.81	1.21×10^5	1.17×10^5
	3.18	1.19×10^5	
	2.54	1.16×10^5	
Mixing	5.08	1.10×10^5	1.10×10^5
	3.81	1.13×10^5	
	3.18	1.12×10^5	

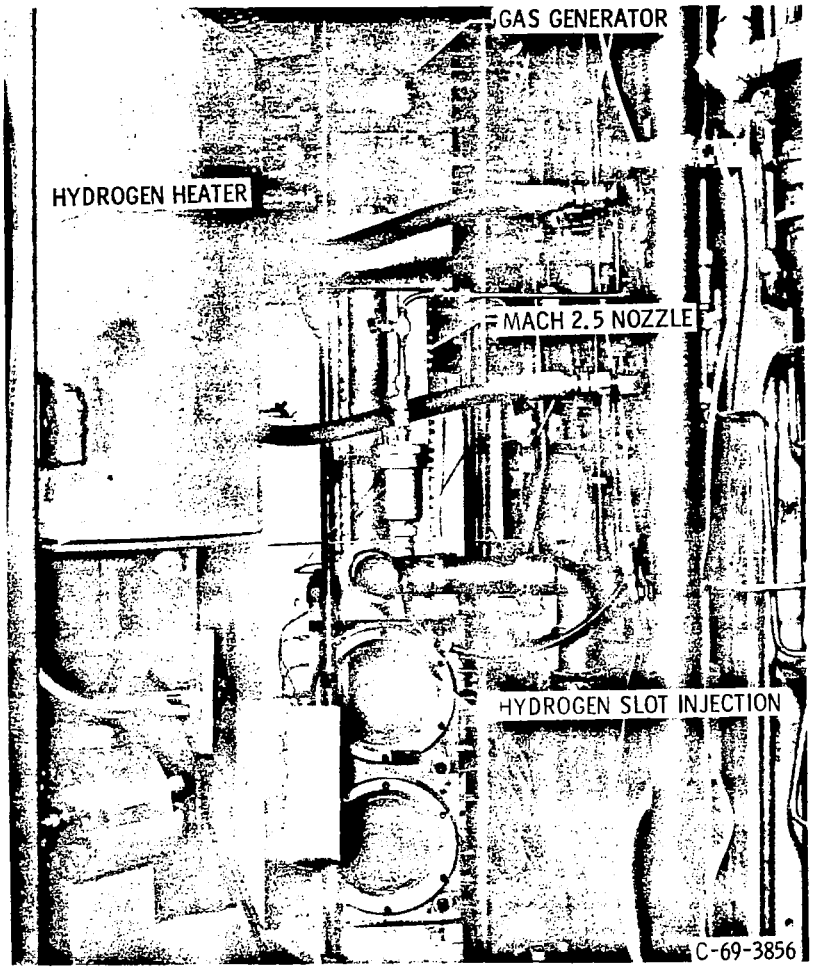

Figure 1. - Supersonic combustion hardware.

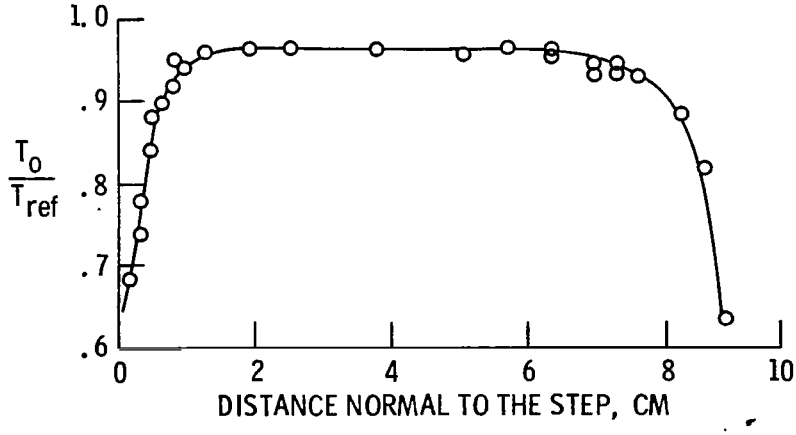

Figure 2. - Total temperature ratio at the injection step, vitiated air.

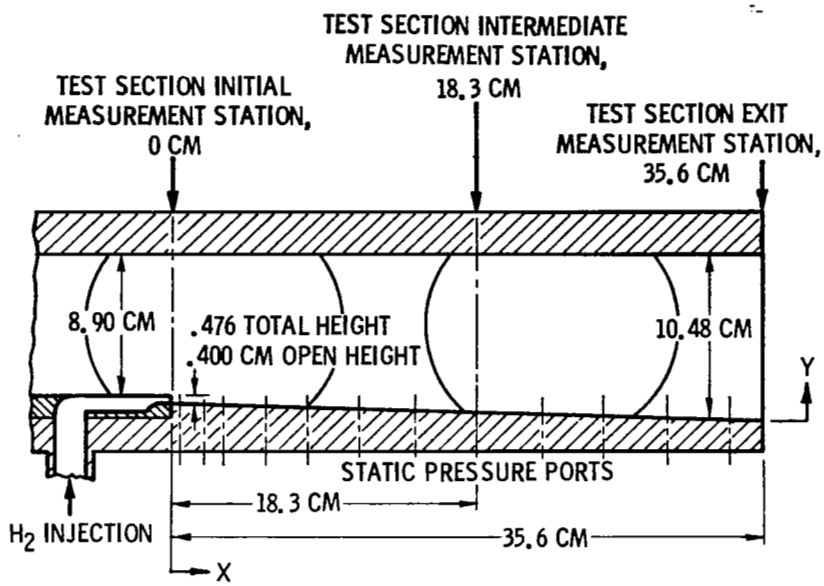

Figure 3. - Test section showing hydrogen injection step, location of static pressure ports and measurement stations.

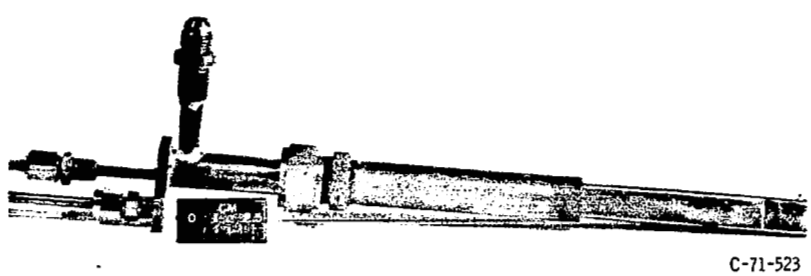

Figure 4(a). - Thermocouple probe.

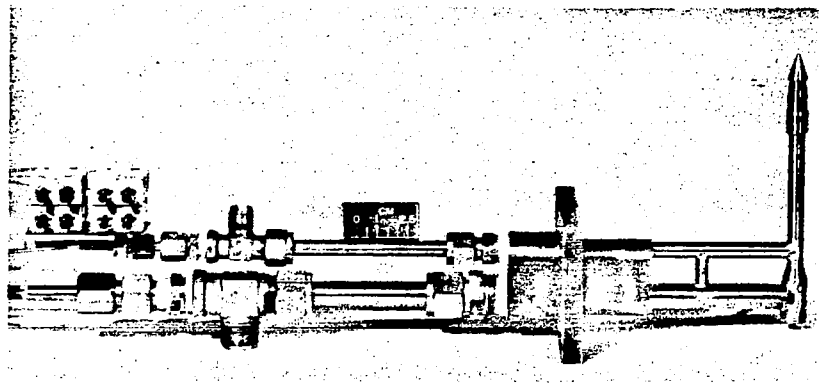

C-71-524

Figure 4(b). - Sample probe II.

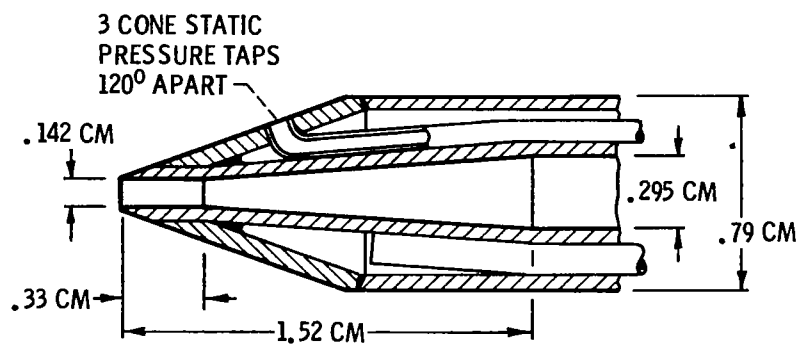

(A) PROBE I TIP DESIGN - CLOSED CIRCUIT COLD WATER COOLING AT 5.34×10^6 N/m^2 PRESSURE

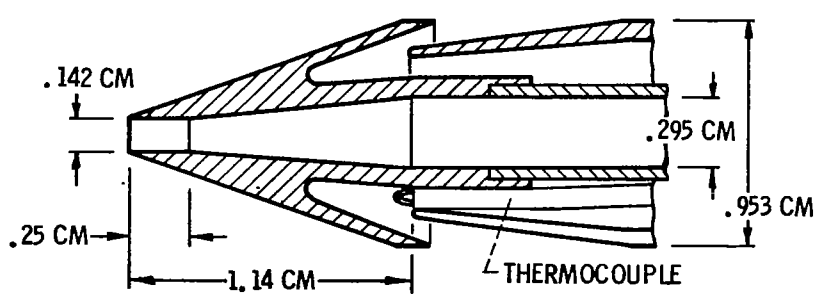

(B) PROBE II TIP DESIGN - OPEN CIRCUIT HOT WATER COOLING AT 1.72×10^6 N/m^2 PRESSURE

Figure 5. - Sampling probe tip details.

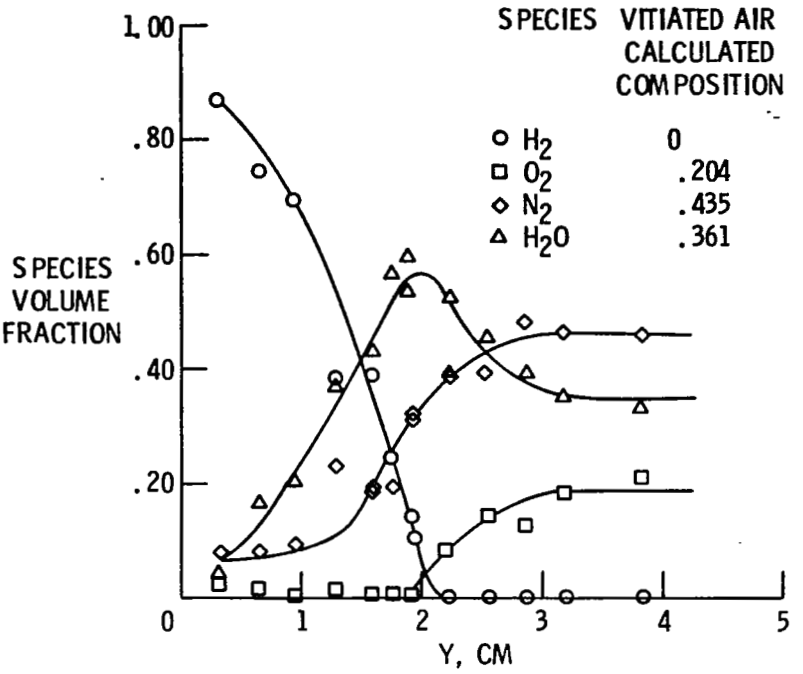

Figure 6. - Composition profile using probe I.
X = 35.6 cm, hydrogen-vitiated air.

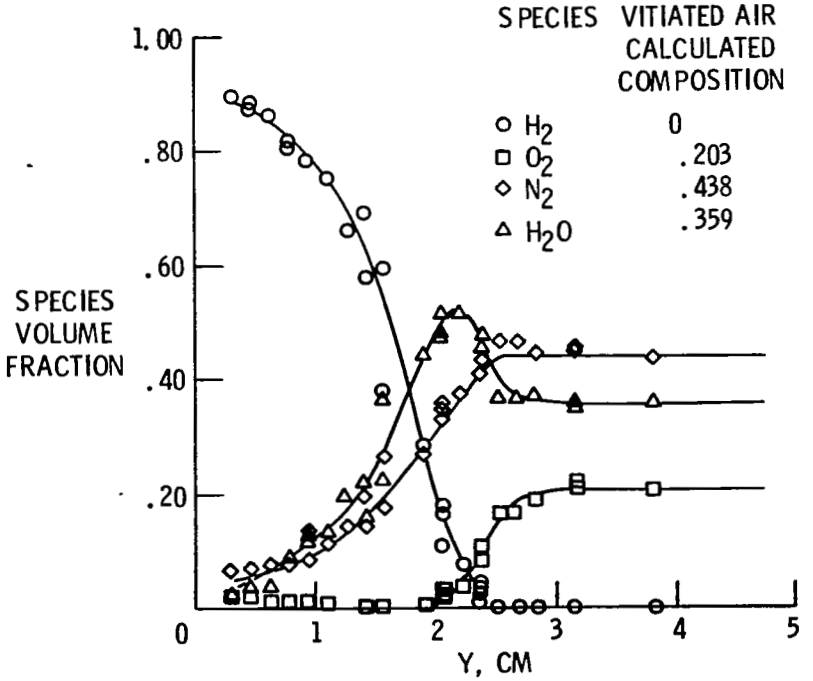

Figure 7. - Composition profile using probe II.
X = 35.6 cm, hydrogen-vitiated air.

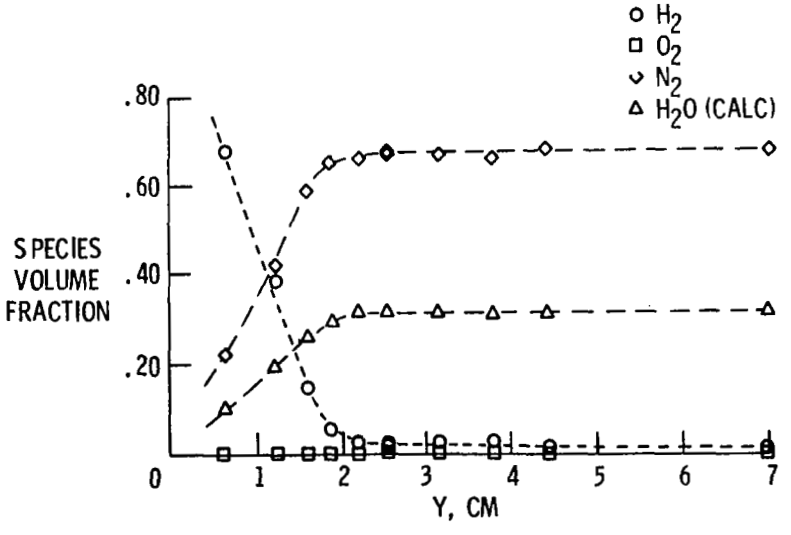

Figure 8. - Composition profile for pure mixing using pitot pressure probe. X = 35.6 cm, hydrogen-inert gas.

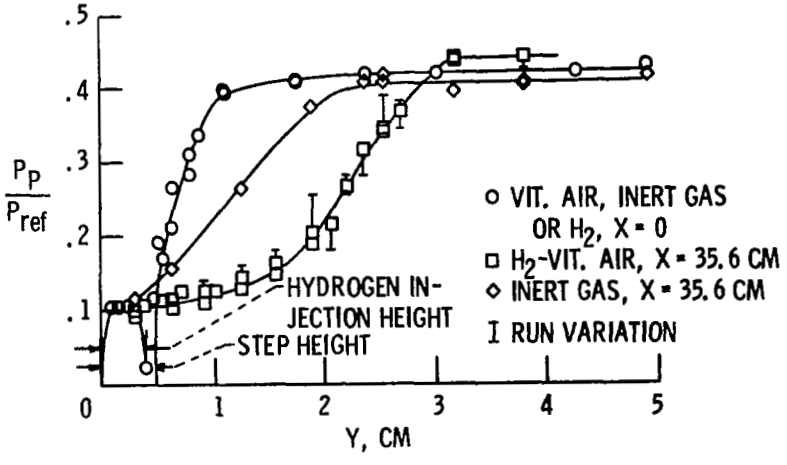

Figure 9. - Pitot pressure profiles. Vitiated air, P_{ref} = 17.1x10^5 N/m^2; inert gas, P_{ref} = 18.5x10^5 N/m^2.

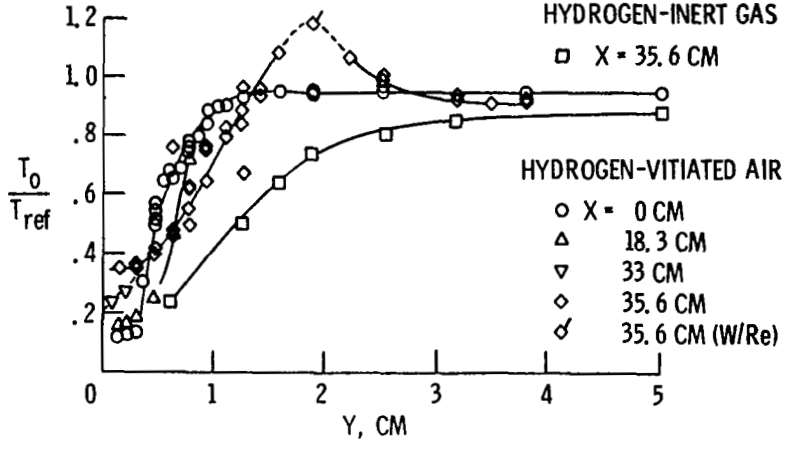

Figure 10. - Total temperature ratios from thermocouple measurements. Vitiated air, T_{ref} = 2380 K; inert gas, T_{ref} = 2276 K.

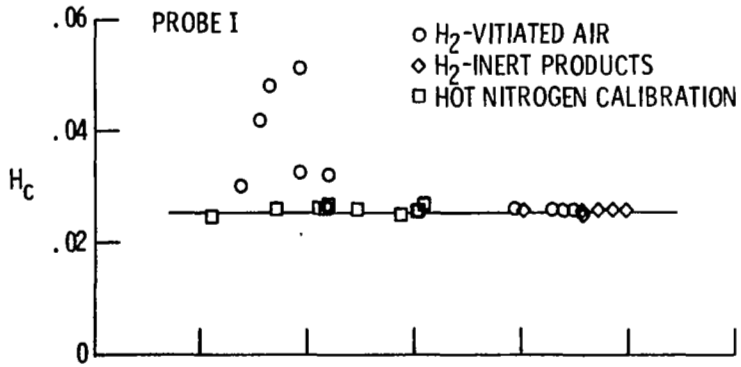

(a) $H_c = St \cdot Re^{0.175} \cdot Pr^{0.667}$.

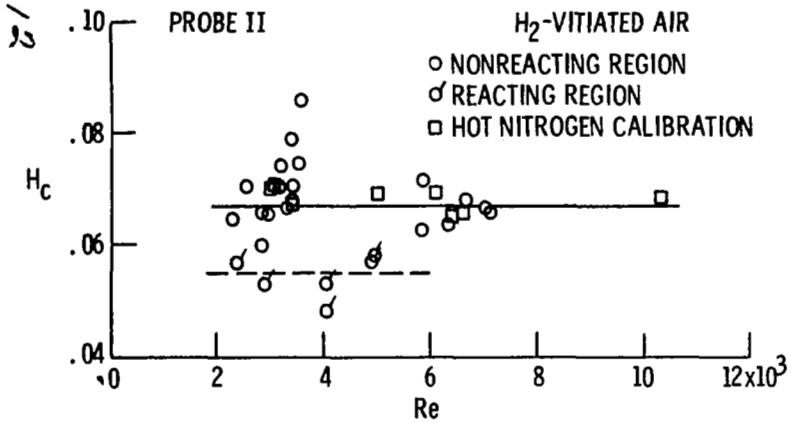

(b) $H_c = St \cdot Re^{0.275} \cdot Pr^{0.667}$.

Figure 11. - Heat transfer calibrations of probes I and II.

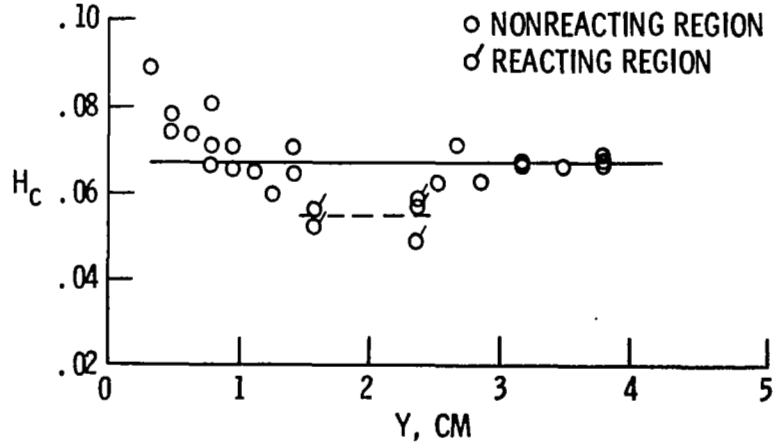

Figure 12. - Calibration constant H_c versus distance Y. Hydrogen-vitiated air.

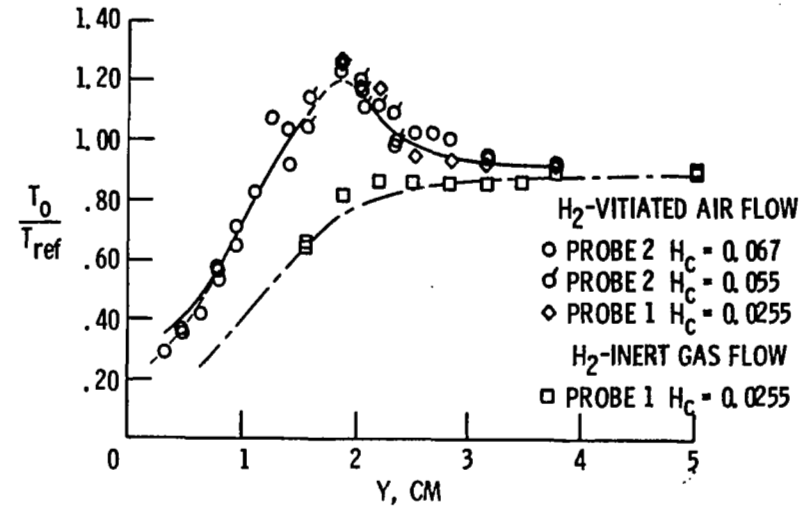

Figure 13. - Total temperature ratio from cooled-gas pyrometer measurements, X = 35.6 cm; vitiated air, T_{ref} = 2380 K; inert gas, T_{ref} = 2276 K.

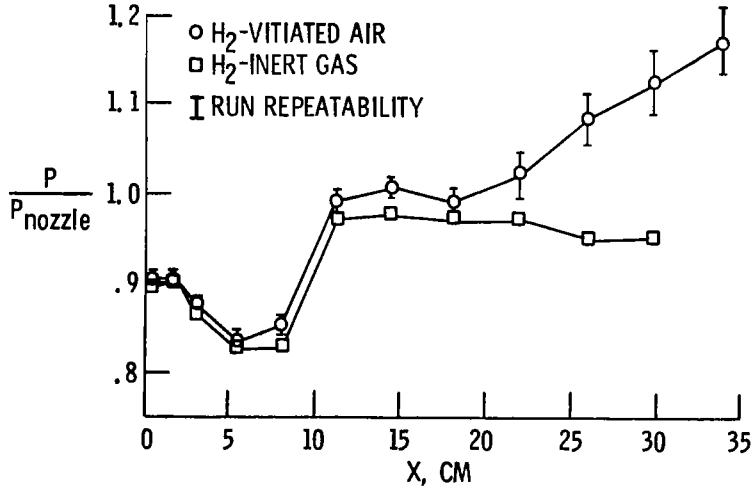

Figure 14. - Wall static pressure ratio. $P_{nozzle} = 0.917 \times 10^5$ N/m^2.

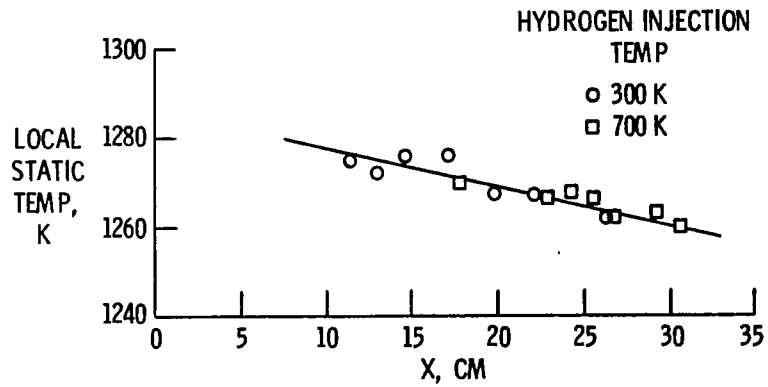

Figure 15. - Hydrogen-vitiated air ignition distances determined by onset of ultraviolet radiation.

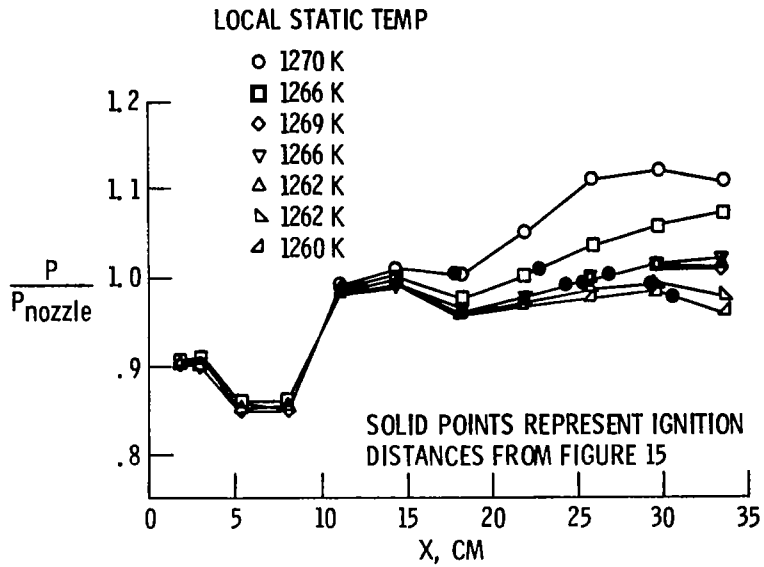

Figure 16. - Wall static pressure for various local static temperatures; total temperature of hydrogen, 700 K.

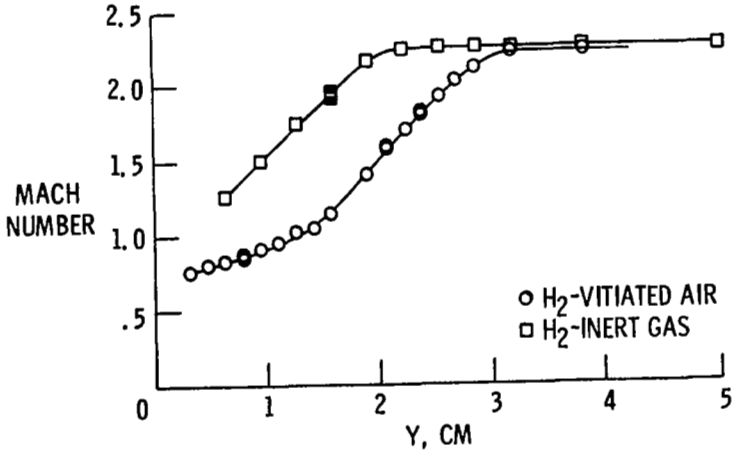

Figure 17. - Mach number profile. X = 35.6 cm.

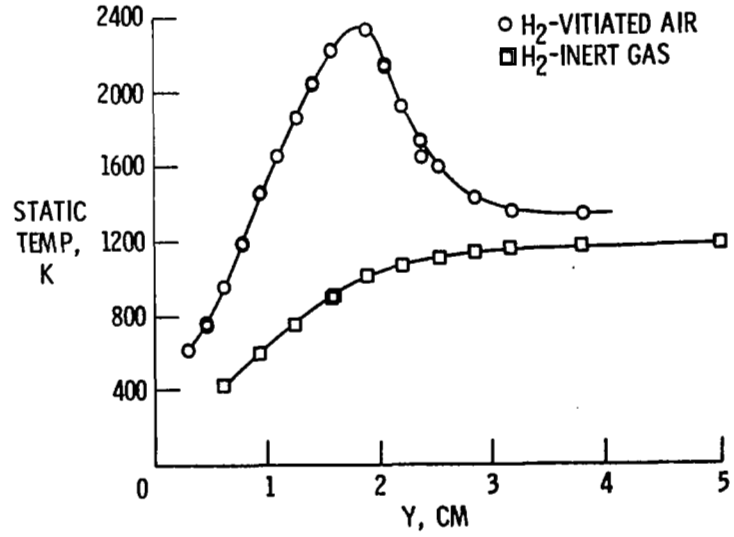

Figure 18. - Static temperature profile. X = 35.6 cm.

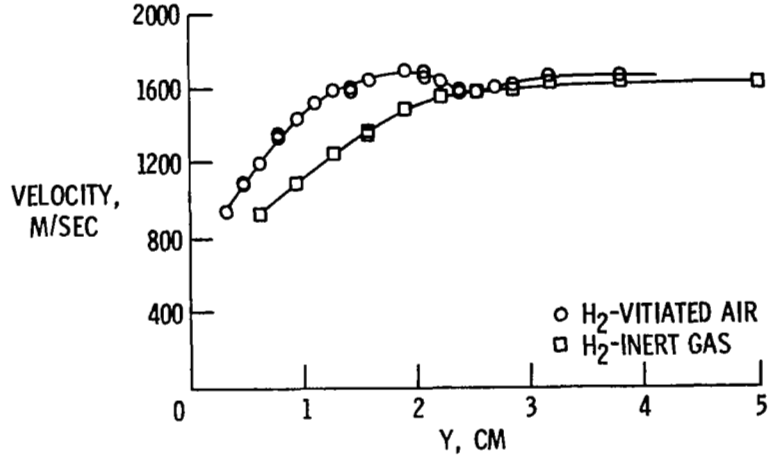

Figure 19. - Velocity profiles, X = 35.6 cm.